Simulating the Effects of Irrigation over the U.S. in a Land Surface Model

Based on Satellite Derived Agricultural Data

Mutlu Ozdogan[1]*, Matthew Rodell[2], Hiroko Kato Beaudoing[2,3], and David L. Toll[2]

*corresponding author

[1]Center for Sustainability and the
Global Environment (SAGE)
University of Wisconsin
Madison, WI, 53706
ozdogan@wisc.edu

[2]Hydrological Sciences Branch
NASA Goddard Space Flight Center
Greenbelt, MD 20771

[3]Earth System Science
Interdisciplinary Center (ESSIC)
University of Maryland
College Park, MD 20742

submitted to

Journal of Hydrometeorology

April 2009

Abstract

A novel method is introduced for integrating satellite derived irrigation data and high-resolution crop type information into a land surface model (LSM). The objective is to improve the simulation of land surface states and fluxes through better representation of agricultural land use. Ultimately, this scheme could enable numerical weather prediction (NWP) models to capture land-atmosphere feedbacks in managed lands more accurately and thus improve forecast skill. Here we show that application of the new irrigation scheme over the continental US significantly influences the surface water and energy balances by modulating the partitioning of water between the surface and the atmosphere. In our experiment, irrigation caused a 12 % increase in evapotranspiration (QLE) and an equivalent reduction in the sensible heat flux (QH) averaged over all irrigated areas in the continental US during the 2003 growing season. Local effects were more extreme: irrigation shifted more than 100 W/m² from QH to QLE in many locations in California, eastern Idaho, southern Washington, and southern Colorado during peak crop growth. In these cases, the changes in ground heat flux (QG), net radiation (RNET), evapotranspiration (ET), runoff (R), and soil moisture (SM) were more than 3 W/m², 20 W/m², 5 mm/day, 0.3 mm/day, and 100 mm, respectively. These results are highly relevant to continental- to global-scale water and energy cycle studies that, to date, have struggled to quantify the effects of agricultural management practices such as irrigation. Based on the results presented here, we expect that better representation of managed lands will lead to improved weather and climate forecasting skill when the new irrigation scheme is incorporated into NWP models such as NOAA's Global Forecast System (GFS).

1. Introduction

Land surface conditions govern moisture, heat, and momentum exchanges between the surface and atmosphere, greatly influencing global weather patterns that further affect our society. By modulating surface-atmosphere exchanges of heat and water, agricultural land management can significantly influence the climate system and the hydrological cycle (Bonan 1997; Bonan 2001; Stohlgren et al. 1998; Chase et al. 2000). In particular, cropland irrigation has been shown to affect local and regional climates and hydrology by modifying the partitioning of water between the surface and the atmosphere (Pielke and Zang, 1989; Otterman et al. 1990; Ben-Gai et al. 2001; Moore and Rojstaczer 2002; Ozdogan et al. 2006; Lobell and Bonfils, 2008; Kueppers et al. 2008; Lobell et al., 2008). At larger scales, however, the climatic and hydrologic effects of irrigated croplands are still poorly understood.

Numerical weather prediction (NWP) and climate models have adopted progressively more sophisticated representations of land surface processes over the course of past two decades (e.g., Dickinson et al. 1986; Sellers et al. 1996; Bonan et al. 2002; Ek et al. 2003). These land surface models (LSMs) simulate the behavior of complex and highly variable (in both space and time) surface states such as soil moisture, temperature, and snow water and provide initial and updated conditions to simulations of large-scale atmospheric processes. However, despite progressive improvement of input variables, treatment of vegetation, and soil physics, today's LSMs largely ignore the effects of irrigation and other land management practices on an operational basis. Herein we describe an original technique for applying satellite derived irrigation data and high resolution crop type information within a LSM, and evaluate its effects on modeled land surface states and fluxes. With the research presented here, our objective is

two-fold: to assess the effects of irrigation and land management on LSM derived states and fluxes; and to improve representation of managed lands in land surface schemes.

2. Background

A number of studies used numerical model simulations to study the effects of irrigation within both uncoupled and coupled (from the atmosphere) experiments. The majority of uncoupled experiments concentrated on irrigation's influence on hydrological fluxes and states. For example, Mahmood and Hubbard (2002) investigated the effects of irrigated agriculture on near-surface hydrological cycle components using a simple soil moisture model. They found that irrigated croplands impart much more water to the atmosphere via evapotranspiration than natural grasslands in unaltered landscapes. In another uncoupled study, de Rosnay et al. (2003) showed that intensive irrigation has a regional impact on the partitioning of energy between sensible and latent heat fluxes and pointed out that irrigation can be a major factor in the water cycle. Their model was developed to take into account the interactions between water demand and land and atmospheric processes, which together define water availability. Haddeland et al. (2006) developed an irrigation scheme for the Variable Infiltration Capacity (VIC) LSM based on simulated soil moisture deficit. Application of the scheme to the Colorado and Mekong river basins showed that in general, irrigation leads to decreased streamflow and increased evapotranspiration. They also demonstrated that while increases in basin averaged latent heat flux were small, irrigation caused locally significant increases (up to 60%) in evapotranspiration which reduced surface temperatures, and hence decreased sensible heat flux. More recently, Tang et al (2007) investigated the effects of natural and anthropogenic heterogeneity (including irrigation) on a hydrological simulation using a distributed biosphere hydrological model system.

The results suggest that irrigation leads to increased evapotranspiration, decreased runoff, increased surface soil moisture, and decreased streamflow. In concert with previous studies, while the average latent heat flux in the peak irrigation season increased only slightly, maximum simulated increase in the latent heat flux exceeded 40 W/m^2 with a strong consequence of ground temperature decrease.

Irrigation has also been studied in coupled modeling experiments. Early coupled experiments simply kept a portion of land surface wet under idealized conditions (Yeh et al. 1984). Recent experiments have been more sophisticated. For example, Segal et al. (1998) used a top-down approach to irrigation, imposing a fixed amount of evapotranspiration from irrigated lands under ideal conditions during the growing season in order to assess feedbacks to summer precipitation. Results indicated that the effects of irrigation on rainfall are mostly non-local, and that irrigation is more likely to augment existing weather systems than trigger new ones. In an irrigation impact study using the Colorado State University Regional Atmospheric Modeling System (RAMS), Adegoke et al. (2003) found significant differences in the regional average surface energy fluxes between the control (irrigated) and the dry (non-irrigated) experiments in central Nebraska. Monthly mean and daily maximum temperatures for the irrigated site steadily decreased during the growing season in contrast to an increasing trend at the non-irrigated site. Chen and Avissar (1994) investigated the formation of meso-scale circulations induced by landscape discontinuities, specifically in the form of dry and wet patches that are present in irrigated areas, and concluded that these circulations are strongly related to the variability of meso-scale heat fluxes into the planetary boundary layer. Thus, to capture cloud development, radiation balance, and other boundary layer processes in atmospheric models, their study suggested that the locations and patterns of landscape heterogeneities, patterns of irrigation in

particular, should be represented in coupled models. More recently, Kueppers et al (2007) used a regional climate model to show that irrigation can have cooling effect in the dry season and concluded that in California "past expansion of irrigated land has likely affected observations of surface temperature, potentially masking the full warming signal caused by greenhouse gas increases." Kueppers et al (2008) also reported on the seasonally varying temperature responses of four regional climate models to irrigated agriculture development in the western US. Overall, irrigation produced large decreases in air temperature and large increases in relative humidity in mid summer months but different models had varying responses to irrigation. Similarly, Kanamaru and Kanamitsu (2008) examined the mechanisms of nighttime minimum temperature warming in the California during summer due to irrigation and concluded that ground heat flux efficiently keeps the surface warm during nighttime due to increased thermal conductivity of wet soil. Finally, Weare and Du (2008) explored the influences of global warming and land use changes on past climate change in California and conclude that summer that irrigation has a strong effect on the differences between recent and past conditions in maximum temperature, surface latent and sensible heat fluxes, surface moisture, and surface humidity.

As evident in their nature, previous studies on irrigation within numerical models tend to fall into two categories: uncoupled, small scale and more realistically parameterized experiments at local scales (e.g. Haddeland et al., 2006), and coupled, larger scale experiments with highly simplified representations of irrigation (e.g. Lobell et al. 2006). The advantages of the latter are ease of implementation and computational efficiency, at the expense of realism. Here we introduce a realistic yet portable irrigation scheme and demonstrate its efficacy in a land surface model (Noah) that is used operationally for (coupled) weather prediction. A major advantage of the new scheme is its implementation at a nearly continental scale based on an accurate, satellite

derived map of irrigation intensity, as well as its operation status within numerical weather prediction models.

3. Data

3.1 Satellite Derived Irrigation Intensity

The primary objective of this study is to quantify the effects of irrigation on land surface states (e.g., soil moisture and temperature) and fluxes (e.g., evapotranspiration and runoff) by implementing a realistic irrigation scheme within an uncoupled land surface model. The first requirement to achieve this objective is an accurate, objective, contemporary map of irrigation intensity and extent. Most existing irrigation maps were compiled from county level statistics which are often outdated (Siebert et al. 2007), or were produced using coarse resolution satellite data (Thenkabail et al. 2008). Even in regions such as the U.S., where irrigation statistics are generally reliable and well documented the disparate information cannot be easily synthesized into a single continental scale database. To overcome these limitations, this research utilizes a new high spatial resolution irrigation dataset derived from satellite observations. The details of the new dataset are provided by Ozdogan and Gutman (2008). In short, the dataset was generated by merging gridded climate datasets and remotely sensed observations from the MODerate resolution Imaging Spectroradiometer (MODIS) instrument aboard NASA's Terra satellite within an image classification algorithm. The new dataset is objective, accurate, and characterizes the distribution of per-pixel fractional area of irrigated lands in the continental U.S. *circa* 2001 at relatively high (500-meter) spatial resolution.

3.2 Land-Cover

The land cover classification dataset used in the experiments was generated by merging gridded land cover and crop type distribution databases. The land cover database is a static, 1 km resolution, global map of land cover classes produced at the University of Maryland (UMD) based on observations from the Advanced Very High Resolution Radiometer (AVHRR) aboard the NOAA-15 satellite (Hansen et al. 2000). The UMD classification scheme includes eleven vegetation classes, bare ground and urban land cover classes, and water. While the UMD land cover map includes a "cropland" land cover class, it does not distinguish different crop types, let alone the irrigation status of those crop types. In reality, each type of crop has distinct irrigation water requirements and timing, which vary with the climate. Using an average crop type in an irrigation simulation scheme could cause grossly over- or under-estimated water input. To remedy this issue, we developed a new global dataset, which categorizes crop type distributions within the UMD land cover map. The basis for crop categorization was a crop type database (hereafter CROPMAP) which consists of 5 min (~10 km) resolution maps of the distributions of 19 different crops, where each crop type layer describes that crop's intensity at each pixel as a percentage of all crops (Leff et al. 2004). CROPMAP is a synthesis of crop specific agricultural census data and spatially explicit data on the extent of the world's croplands. It represents a first order global database that is generally consistent with common agricultural knowledge and is also largely consistent with U.S. Department of Agriculture reports.

To generate a gridded land cover map, which includes information on specific crop types, we merged the UMD map with the CROPMAP as follows. For every 5-min CROPMAP grid, we applied the appropriate percentage distribution of the 19 crops to the roughly one hundred 1 km UMD "cropland" pixels randomly space. For example, within a CROPMAP cell that

contained 60 percent maize and 40 percent soy, we randomly assigned 60 of the corresponding UMD cropland pixels to maize and 40 to soy. In cases of inconsistency between the two datasets, the UMD classification took precedence. That is, when the UMD dataset had no crop pixels in a given 5-min cell, no crops types were imposed regardless of the CROPMAP information. When the UMD map indicated that crops existed but CROPMAP did not, UMD "cropland" pixels were prescribed as wheat, reasoning that wheat is the most widespread crop type in the U.S. Inconsistencies between the two datasets were infrequent and thus not a significant source of error. To quantify the rate of inconsistency, the newly generated 1 km land cover map was aggregated to 5-min spatial resolution, and in all cases the percentage of crop types was within 5% of that reported in the original CROPMAP dataset.

The new land cover database is a single layer dataset with ~1 km spatial resolution, representing 31 land cover classes (12 UMD land cover classes + 19 crops). To meet the input requirements of the Land Information System model driver (LIS; described in detail section 4.1), the merged 1 km dataset was aggregated to a 0.125° model grid by counting the number of pixels of each land cover class in each 0.125° grid square.

3.3 Meteorological Forcing

The North American Land Data Assimilation System (NLDAS) forcing dataset (Cosgrove et. al. 2003) was used to drive the simulations. The dataset covers the continental United States and parts of Canada and Mexico [125°W-67°W, 25°N-53°N] at 0.125° and hourly resolutions. It consists of numerical weather prediction model outputs and observation based products which are blended and interpolated to the required resolutions. The baseline forcing fields are generated by the NCEP Eta Data Assimilation System (EDAS; Rogers et al. 1996) or

the Eta model when EDAS is not available. The precipitation and radiation fields are replaced by observation based data as available. The NOAA Climate Prediction Center (CPC) daily gauge data (Higgins et al. 2000) are downscaled to hourly resolution using Stage II Doppler radar data (Baldwin and Mitchell 1997). The downward shortwave radiation data are derived from Geostationary Operational Environmental Satellite (GOES) observations (Pinker et al. 2003). An elevation adjustment is applied to the surface pressure, longwave radiation, 2 m temperature, and humidity fields to account for discrepancies in topography between EDAS/Eta and NLDAS due to their differing spatial resolutions.

4. Methods

4.1 Land Surface Model and Driver

Experiments were performed with the Noah LSM (version 2.7) running within the Land Information System (LIS). LIS is a highly efficient and parallelized model driver which allows users to run multiple LSMs locally to globally, at various resolutions (from 1 km to 2.5°), using a variety of forcing options, from a common software interface (Kumar et al. 2006). LIS has its roots in the North American and Global Land Data Assimilation Systems (NLDAS, Mitchell et al. 2004; GLDAS, Rodell et al. 2004), which have since adopted the LIS software. LIS divides grid pixels into "tiles" based on land cover in order to simulate sub-grid scale heterogeneity, hence the requirement for a high resolution land cover (and crop) database. LIS/Noah proceeds as a series of single column simulations on the sub-grid tiles with no horizontal interactions. Soil texture is based on the United Nations Food and Agriculture Organization (FAO) soil database (Reynolds et al. 2000). Elevation parameters are derived from a global, 30 arc second resolution topographic map (Gesch et al. 1999). LIS is fully modularized and compliant with

Earth System Modeling Framework (ESMF) and Assistance for Land surface Modeling Activities (ALMA) standards, making it an ideal platform for developing innovative modeling and assimilation capabilities, including simulated irrigation.

The Noah LSM (Chen et al. 1996; Koren et al. 1999) was developed beginning in 1993 through a collaboration of investigators from public and private institutions, spearheaded by NOAA's National Centers for Environmental Prediction (NCEP). Noah is a stand-alone, 1-D column model which can be executed in either coupled or uncoupled mode. The model applies finite-difference spatial discretization methods and a Crank-Nicholson time-integration scheme to the equations that describe the physical processes of the soil, vegetation, and snowpack. Outputs are the stocks and fluxes of the near-surface water and energy budgets. Noah has been used operationally in NCEP models since 1996, and it continues to benefit from a steady progression of improvements (Betts et al. 1997; Ek et al. 2003).

4.2 Simulating Irrigation

The three key aspects of irrigation in a modeling framework are the irrigation trigger (when to irrigate), amount (how much to irrigate), and the method (e.g., rain, spray, drip; and rate). In the United States and much of the modernized world, farmers often use 30-40 cm soil moisture sensors to assess plant available moisture in the upper root zone, and irrigate when soil moisture falls below a prescribed threshold. Farmers without moisture sensors either use traditional indicators of soil dryness (e.g., soil color, wilting) or irrigate on a set schedule over periods lacking sufficient rainfall.

Following actual irrigation practices in the US, in our scheme irrigation is triggered when the root zone soil moisture falls below a threshold, in essence replicating a moisture sensor

scenario. The root zone moisture availability (MA) is defined as ratio of the difference between the current root zone soil moisture (SM) and the wilting point, (SM_{WP}) and the difference between field capacity (SM_{FC}) and SM_{WP}:

$$MA = (SM - SM_{WP}) / (SM_{FC} - SM_{WP}) \tag{1}$$

Field capacity (the maximum amount of water that the unsaturated zone of a soil can hold against the pull of gravity) is a parameter that Noah prescribes based on soil type. We chose 50% of field capacity as the irrigation trigger threshold based on discussions with local experts in Nebraska and California followed by trial and error (not shown). The depth of the root zone varies in time according to the plant's growth cycle. Maximum root depth values were assigned based on published coefficients, replacing Noah's default values, and they are used in the calculations of 'current' soil moisture availability. By scaling the maximum root depth with the greenness fraction, the seasonal variability in the root zone is captured. This is necessary because growing season consumption and utilization of water by a crop is largely determined by the expansion of leaf area (represented by greenness fraction) and root depth during phenological development. Hence, phenological development influences transpiration rates, the soil wetness profile, and the water and energy balances.

The irrigation scheme begins by checking if the current tile represents cropland or another potentially irrigated land class (e.g., grass), and whether or not the encompassing grid cell is irrigated. The scheme then determines if it is the growing season. The growing season begins and ends when a threshold of 40% of annual range of greenness fraction at the grid cell is crossed. Most agricultural areas in the U.S. have growing seasons between April and October,

but some locations in the Southwestern U.S. have elongated growing seasons which begin earlier. Next, if MA is below the irrigation trigger, the scheme computes the irrigation requirement for each subgrid tile as an equivalent height of water by subtracting the current root zone soil moisture from the field capacity. If the ratio of irrigated area to total crop coverage in the encompassing grid cell is less than one, then the irrigation requirement for each tile is reduced by the same ratio. Conversely, if that ratio is greater than one, then the tile-area-weighted grid cell total irrigation requirement is scaled up by the ratio, and the additional water is first applied to grassland, if such a tile exists. Any remaining water (beyond the field capacity of the grassland tile) is applied evenly to other non-crop tiles, excluding forests, bare soil, and urban tiles. This approach was chosen primarily to account for misclassification of agricultural areas, based on our assumption that the irrigation map is more reliable than the land cover map. We surmised that distinguishing grassland from cropland using satellite imagery would be especially prone to error. Further, in the cases of golf courses, sod farms, and perhaps other land uses, grass and irrigation are not mutually exclusive. To illustrate the approach, given a grid cell with 60% irrigation intensity and wheat, soy, grassland, and forest tiles covering 30%, 20%, 40%, and 10% of its area, each at 10 mm below field capacity, the scheme would apply 10 mm irrigation to the wheat and soy tiles and [10 mm * (60% - 30% - 20%) / 40%] = 2.5 mm to the grassland tile. In this example, a uniform 10 mm requirement is used for the sake of simplicity. In actuality, root zone depth varies by land cover type and greenness fraction, so crop tiles are likely to have different irrigation requirements.

The irrigation trigger is evaluated daily at 6:00 am local time. If positive, the irrigation requirement is applied as precipitation (i.e., sprayed from above) at a uniform rate between 6:00 am and 10:00 am, a timeframe typically chosen by farmers to reduce evaporative losses. Other

than the efficiency, the resulting states and fluxes are not likely to differ much from an algorithm that applies the irrigation directly to the soil since we allow some water to evaporate and runoff before it starts percolating through soils, as what would happen in spray irrigation. A preliminary test (not shown) of applying water directly to soil moisture resulted in too much irrigation water for the US Midwest, which may be partially explained by pressure (spray) irrigation being the most common method of water delivery in the country. The irrigation scheme is invoked at each (15 minute) time step before the LSM is called. We assumed that water resources are freely available for irrigation (i.e., from surface or ground waters - reservoirs which are not simulated in Noah 2.7.1). Further, the amount applied is effectively the net irrigation, i.e., after on the field and transportation losses.

4.3 Experimental Design

Three experiments were performed to assess the impact of agricultural land management on hydrological fluxes: *control*, *crops*, and *irrigation*. Both the *crops* and *irrigation* experiments used the new UMD-CROPMAP dataset, while *control* used the original UMD dataset with a single "average" crop class. No irrigation was applied in the *control* and *crops* experiments. The new crop map (*CROPMAP*) was required for the scheme to determine how much irrigation to apply to a given irrigated area. The purpose of the *control* experiment was to isolate the impact of adding a realistic array of crop types. That impact turned out to be minor (i.e., the *control* and *crops* experiments produced similar results), hence the *control* experiment will not be discussed in detail in the remainder of this paper. The impact of irrigation is demonstrated through comparisons between the *crops* and *irrigation* experiments. The effective domain was the continental US, gridded at 0.125° resolution, and the experimental period was 2003. The 1-

km UMD and UMD-CROPMAP datasets were used to define sub-grid tiles. In all experiments, a minimum grid coverage threshold of 5% was assigned in determining the number and types of tiles, i.e., vegetation classes that covered less than 5% of a given grid cell were not modeled. The vegetation parameter file in Noah was augmented with the new values for the 19 crop types. Some of these parameters (e.g., root depth and roughness length) are physical and were acquired from the literature, while others are non-physical and specific to the Noah model, making them difficult to estimate. For example, in the *control* experiment, root depth for the average crop class extends to layer 3 and roughness length is 0.035m. In the *crops* and *irrigation* experiments with explicit crop types, some crops have root depth extending beyond the third soil layer and roughness lengths are higher than 0.035m as in the average crop. However, for some of the latter type we used Noah's value for "cropland" land cover as the default. The model time step was 15 minutes and output was recorded hourly. The model was spun-up from 1996 to 2002 using the NLDAS forcing data.

In addition to the three national-scale experiments, two sets of single grid cell ("point") simulations using the same *crops* and *irrigation* schemes were performed for comparison with field data. These data were collected at an irrigated maize site in Mead, Nebraska [41.17°N, 96.48°W] which is part of the AMERIFLUX observational network, and at an irrigated grassland site in Five Points, California [36.34°N, 120.11°W], which is maintained by the USDA. Each point simulation was forced by NLDAS data, with the same spin-up procedure previously described. They differed from the national scale simulations in that they included only a single tile whose land cover type matched that at the field site, and the Five Points simulation continued through 2004 and 2005, the two years for which data were available for that site.

5. Results

5.1 Irrigation water requirements

Accurately representing the amount, location, and timing of water applied is essential for simulating irrigation and quantifying its impact on hydrological fluxes and state variables. Comparison of our predicted irrigation requirements with those compiled for the U.S. at the county level (Hutson 2004) demonstrates that there is generally good agreement between reported irrigation and that applied by our scheme, both in terms of spatial extent (Figure 1) and amount (Figure 2). The root mean square error is less than 0.3 km^3/yr per county, which is reasonable given that the satellite data do not directly indicate the volume of water irrigated. Further, the scheme exhibits low bias (0.012 km^3/yr), which gives us confidence in its ability to simulate real world irrigation both in terms of location and amount. Note that our simulation year (2003) and the reported estimates form the USGS (2000) are not from the same year. Given interannual climate variations, it is likely that these two datasets do not represent the same irrigation amount values. However, comparison of the USGS values to the USDA 2003 Farm and Ranch Irrigation Survey (USDA 2004) (not shown) at the state level yields comparable estimates of irrigation water and thus lends credibility to our comparisons.

Averaged over the entire country, irrigation peaks in July and August, driven by strong summer insolation, high temperatures, and maturing crops in three different regions (Figure 3). This seasonal cycle predicted by the irrigation scheme is intuitive and is corroborated by reported irrigation totals (USDA 2004). Irrigation requirements are a function of crop types and climate, which vary across regions. Model predicted volume of irrigation water is largest in the central region [110°-95°W] and slightly less in the western region [124°-110°W] and this volume is the smallest in the east [95°-67°W]. This is in contrast to the reported irrigation quantities from the

USDA (2004) shown as gray horizontal bars on Figure 3, which suggests higher irrigation volumes in the western region than in the central region. We explain this inconsistency between reported and estimated irrigation volumes by the coarse nature of the greenness fraction data, which effects the timing of irrigation as well as lack of model's ability to capture high water demand agriculture such as vegetables in the western region (mainly in the state of California). Nevertheless, this under- and over-estimation of irrigation volumes does not minimize the main statement of our findings that suggest that irrigation greatly influences the water and energy budgets of the land surface that are so important for land-atmosphere interactions and local climate.

With respect to the timing of irrigation, in the western U.S., irrigation demand shows relatively little high frequency variability, increasing quickly from May through early July and then gradually decreasing through October. The most heavily irrigated area in the west is California's Central Valley, which is dominated by vegetables and orchards with extended growing seasons. The dominant crop in the northern part of the western region is wheat. Western agriculture's constant dependence on irrigation, particularly in California, owing to a dry season which extends from May to October, accounts for the relative smoothness of the plot of irrigation rates. Its early peak corresponds with an early peak in greenness fraction, which occurs near the end of June. In the central region, the irrigation rate increases in spring followed by a larger increase throughout summer and a sharp decline in the fall. Here, the dominant crop types are maize and soybeans, which exhibit a strong summer demand for irrigation. In contrast, the eastern region typically has much lower irrigation demand because of its more humid climate.

5.2 Irrigation effects on energy and water budget components

Irrigation raises the soil water content, enabling evapotranspiration, which in turn transforms the energy budget. Simulated increases in evapotranspiration due to the new irrigation scheme are presented in Figure 4 as a series of monthly maps. The temporal and geographical features described in the previous section are evident. In general, peak increases in evapotranspiration occurred in July and August, though the region of heavy irrigation in the southeastern U.S. along the Mississippi River lagged in phase. In parts of California, Washington, Indiana, Colorado, Nebraska, South Dakota and North Dakota, evapotranspiration increased by at least 100% of the *crops* simulation during the summer peak. In one extreme case, evapotranspiration in a pixel in California jumped from 1.44 mm/month to 177 mm/month.

The majority of current LSMs do not include explicit crop types, thus their "crop" vegetation parameters are meant to be representative of the average. However, explicit description of crop types appears to affect simulation of both water and energy budgets (not shown). Increasing the number of crop types to 19 and specifying new parameters for each generally shifted energy or water balance components in the same direction as simulating irrigation, but to a much lesser amount. However, the mean soil moisture (SM) values in the *control* and *irrigation* experiments were nearly equivalent, while the *crops* means were consistently lower. This highlights the importance of realistically simulating crops, which in the case of the Noah model enables more root uptake and transpiration, and hence results in a drier root zone (in the absence of irrigation).

Averaged over all irrigated areas in the continental U.S. and over the growing season (April to October), irrigation increased latent heat flux (QLE) by 9 W/m² (or 12 % of QLE from *crops*), decreased sensible heat flux (QH) by 8 W/m² (11 %), and slightly increased ground heat

flux (QG) by 0.05 W/m² (2 %) and net radiation (RNET) by 1.2 W/m² (0.8 %). To balance the extra input of water, evapotranspiration (ET) rose by 0.3 mm/day (or 12 % of *crops*), runoff (R) by 0.01 mm/day (5 %), and total column soil moisture (SM) by 15 mm (4 %). As with irrigation itself, these effects were most pronounced in July and August. At their peak in August, QLE and ET increased by 26%, QG by 5%, RNET by 2%, R by 11%, and SM by 7 %, and QH decreased by 18%,.

Diagnostics are included in Figure 5 for the same three regions previously defined: Western, Central, and Eastern U.S. Because Western agricultural regions are relatively arid, on average, they received the most irrigation per unit irrigated area, and accordingly, the effects were greatest. Both irrigation rate and effects were most pronounced in the Central Valley of California, which skewed the Western averages. Save for SM, the effects of increasing crop types were greatest in the Eastern region. Local effects were sometimes extreme. For example, irrigation shifted more than 100 W/m² from QH to QLE in the energy balance of many locations in California in July. In these cases, the changes in QG, RNET, ET, R, and SM were more than 3 W/m², 20 W/m², 5 mm/day, 0.3 mm/day, and 100 mm, respectively. Impacts of similar magnitude were also seen in eastern Idaho, southern Washington, and southern Colorado.

We also compared the ability and outcome of the irrigation module over individual sites for which detailed information exists. One such site is an Ameriflux site near Mead, Nebraska (Figure 6). Here, volumetric soil moisture in the *crops* followed a normal summertime drying trend, interrupted by rainfall events. However, observations from the site indicate that irrigation kept soil moisture near saturation. The scheme predicted irrigation on 11 days, totaling 396 mm of water between July 1 and August 31. This agrees remarkably well with the reported irrigation frequency (12 days) and total (345 mm), despite a few early mismatches between NLDAS and

observed rainfall, which hampered the scheme's ability to predict the exact days when irrigation was applied. Simulating irrigation dramatically increased soil moisture, maintaining it within approximately the same range as that of observed suggesting significant improvements in modeled soil moisture and fluxes with the irrigation scheme (Figure 6).

Presence of irrigation also improved simulated diurnal cycles of latent and sensible heat fluxes at the Mead field site as compared to observations (Figure 7a and 7b). The amplitude of the *crops* latent heat flux at midday was underestimated by about 200 W/m^2, while the sensible heat flux was overestimated by about 340 W/m^2. When the irrigation scheme was engaged, those errors reduced to within 80 W/m^2, and the shape of the diurnal cycle of sensible heat flux greatly improved.

The effects of irrigation in California's central valley are also dramatic. At the Five Points irrigated grassland site, ET was measured using a weighing lysimeter (Vaughan et al., 2007) during 2004 and 2005. The site received no significant accumulation of rain during the summers of those years. Consequently, the *crops* experiment generated dry soils and near zero ET in August of both years (Figures 7c and 7d). When the irrigation scheme was activated, the additional moisture enabled Noah's diurnal cycle of ET to approximate the observations reasonably well, with a 15% low bias in 2004 and a 25% low bias in 2005. The irrigation scheme alleviated corresponding high biases in sensible heat flux and surface temperature (not shown).

Similar changes were also evident in the national-scale simulations. While the *crops* experiment overestimated daytime land surface temperature in most irrigated regions, the *irrigation* experiment produced results more consistent with observations based on the following normalized temperature difference metric:

$$\Delta LST_{model\text{-}obs} = |LST_{crops} - LST_{GOES}| - |LST_{irr} - LST_{GOES}| \qquad (2)$$

In (2), LST_{crops} and LST_{irr} refer to land surface temperature predicted by the *crops* and *irrigated* runs respectively and LST_{GOES} is the land surface temperature observed by the GOES instrument. Accordingly, incorporating irrigation with the new scheme decreases the land surface temperature averaged over the 13-day period between August 13 and August 25, 2003 at 18 Z, in essence reducing land surface temperature prediction errors on the order of 10 K when compared to satellite observations (depicted as positive values in Figure 8). Note that due to inherent difficulties in modeling land surface energy balance, there are expected differences between the two surface temperature estimates. However, these differences between GOES and modeled LST are the reason we chose to depict the improvements following equation (2) – these improvements are much easier to see when decoupled from all GOES-model differences. While Figure 8 does show differences over non-irrigated areas, these areas are not relevant to the present study.

6. Discussion

The results demonstrate that irrigation significantly modulates the water and energy budgets of the land surface, in agreement with conclusions of previous studies. The primary innovation of this work is a computationally efficient yet sufficiently realistic irrigation scheme based on satellite observations of irrigation intensity, which has already been implemented over the continental U.S. and which will be straightforward to apply globally once the irrigation intensity map has been extended. It has been shown that by employing a simple set of rules based on actual practices to determine when and how much to irrigate, the scheme reasonably approximates reported irrigation water application rates. This provides a measure of confidence

that the scheme will produce useful results in parts of the world where irrigation data are not available, though it may have to be optimized for crops not grown widely in the U.S., such as rice.

The Noah LSM, used here, is the land component of NOAA's Global Forecast System (GFS; NOAA 2005). It improves the skill of NOAA's short term and seasonal forecasts by simulating the behavior of complex and highly variable (both in space and in time) land surface conditions including soil moisture and temperature, which affect atmospheric stability and boundary layer growth. Many studies have shown that conditions at the land surface in certain regions govern the development of weather patterns and precipitation (e.g., Dirmeyer 2000; Koster et al. 2004). During the growing season in many agricultural regions, irrigation can completely transform the terrestrial water and energy budgets. Therefore we expect that, through improved simulation of land surface conditions, the new irrigation scheme will lead to improved weather and climate forecasting skill when incorporated into NWP models such as NOAA's GFS, especially when we implement a full water balance scheme that will account for irrigation sources. Furthermore, it can easily be adapted for use in other land surface and coupled modeling systems.

The results are also highly relevant to regional to global scale water and energy cycle studies. Irrigated area accounts for 2.7 % of the continental U.S. based on the MODIS derived irrigation map. When averaged over the entire U.S., the water and energy budget effects presented in section 5.2 are diluted accordingly. For example, the nationwide increase in QLE (ET) was 4%. That is still a significant change in the water and energy balances considering the scale. Further, due to the fact that farmers irrigate more in dry months and years, if water is available, irrigation may act to buffer otherwise variable land surface conditions and fluxes,

which would feed back to the evolution of weather patterns and other phenomena such as droughts. Exploring this hypothesis will be an important direction for future work. To date, most continental to global scale water and energy cycle studies have not attempted to quantify irrigation effects. Our results provide a way forward using a modeling approach which can simultaneously incorporate other large scale observations as inputs and constraints, following the LDAS paradigm (Mitchell et al. 2004; Rodell et al. 2004).

References

Adegoke, J.O., Pielke, R.A., Eastman, J., Mahmood, R., and Hubbard, K.G., 2003: Impact of irrigation on midsummer surface fluxes and temperatures under dry synoptic conditions: A regional atmospheric model study of the U.S. High Plains, *Monthly Weather Review*, **131**, 556-564.

Baldwin, M., and Mitchell, K.E., 1997: The NCEP hourly multi-sensor U.S. precipitation analysis for operations and GCIP research, in Preprints, *13th AMS Conference on Hydrology*, pp. 54– 55, Am. Meteorol. Soc., Boston, Mass.

Betts, A., Chen, F., Mitchell, K., and Janjic, Z., 1997: Assessment of the land surface and boundary layer models in two operational versions of the NCEP Eta model using FIFE data. *Mon. Wea. Rev.*, **125,** 2896.

Cosgrove, B. A. and Coauthors, 2003: Real-time and retrospective forcing in the North American Land Data Assimilation System (NLDAS) project, *J. Geophys. Res.*, **108** (D22), 8842, doi:10.1029/2002JD003118.

Chen, F. and Avissar, R., 1994: The impact of land-surface wetness heterogeneity on mesoscale heat fluxes, *Journal of Applied Meteorology*, **33**, 1323-1340.

Chen, F., Mitchell, K., Schaake, J., Xue, Y., Pan, H., Koren, V., Duan, Y., Ek, M., and Betts, A., 1996: Modeling of land-surface evaporation by four schemes and comparison with FIFE observations. *J. Geophys. Res.,* **101** (D3), 7251.

deRosnay, P., Polcher, J., Laval, K., and Sabre, M., 2003: Integrated parameterization of irrigation in the land surface model ORCHIDEE. Validation over Indian Peninsula, *Geophysical Research Letters*, **30**, 1986, HLS-2, doi: 10.1029/2003GL018024.

Dirmeyer, P., 2000: Using a global soil wetness dataset to improve seasonal climate simulation, *J. Clim.,* **13** (16), 2900–2922.

Ek, M. B., K. E. Mitchell, Y. Lin, E. Rogers, P. Grunmann, V. Koren, G. Gayno, and J. D. Tarpley, 2003: Implementation of Noah land surface model advances in the National Centers for Environmental Prediction operational mesoscale Eta model, *J. Geophys. Res.*, **108** (D22), 8851, doi:10.1029/2002JD003296.

Gesch, D.B., Verdin, K.L., and Greenlee, S.K., 1999: New land surface digital elevation model covers the Earth, *EOS, Transactions of the American Geophysical Union,* **80** (6), 69-70.

Haddeland, I., Lettenmaier, D.P., and Skaugen, T., 2006: Effects of irrigation on the water and energy balances of the Colorado and Mekong river basins, *Journal of Hydrology*, **324**, 210-223.

Hansen, M. C., R. S. DeFries, J. R. G. Townshend, and R. Sohlberg, 2000: Global land cover classification at 1km spatial resolution using a classification tree approach. *International Journal of Remote Sensing,* **21,** 1331.

Higgins, R. W., W. Shi, E. Yarosh, and R. Joyce, 2000: Improved United States precipitation quality control system and analysis, NCEP/Climate Prediction Center Atlas, vol. 7, 40 pp., U.S. Dept. of Commerce/Natl. Weather Serv. Natl. Oceanic and Atmos. Admin., Camp Springs, Md.

Hutson, S.S., Barber, N.L., Kenny, J.F., Linsey, K.S., Lumia, D.S., and Maupin, M.A., 2004: Estimated use of water in the United States in 2000: Reston, Va., *U.S. Geological Survey Circular 1268,* 46 p.

Kanamaru, H., and M. Kanamitsu, 2008: Model Diagnosis of Nighttime Minimum Temperature Warming during Summer due to Irrigation in the California Central Valley, *J. Hydrometeor.,* **9,** 1061–1072.

Koren, V., J. Schaake, K. Mitchell, Q. Y. Duan, F. Chen, and J. M. Baker, 1999: A parameterization of snowpack and frozen ground intended for NCEP weather and climate models. *J. Geophys. Res.,* **104,** 19569.

Koster, R.D. and Co-authors, 2004: Regions of strong coupling between soil moisture and precipitation, *Science,* **305** (5687), 1138 – 1140, DOI: 10.1126/science.1100217.

Kueppers, L.M., M. A. Snyder, and L. C. Sloan, 2007: Irrigation cooling effect: Regional climate forcing by land-use change, *Geophys. Res. Lett.*, **34**, L03703, doi:10.1029/2006GL028679.

Kueppers, L.M., M.A. Snyder, L. C. Sloan, D. Cayan, J. Jin, H. Kanamaru, M. Kanamitsu, N.L. Miller, M. Tyree, H. Du, B. C. Weare, 2008: Multi-model comparison of the climate response to land-use change in the western United States, *Global and Planetary Change*, **60**, 250-264, doi:10.1016/j.gloplacha.2007.03.005

Leff, B., Ramankutty, N., and Foley, J.A., 2004: Geographic distribution of major crops across the world, *Global Biogeochemical Cycles*, **18** (1), GB1009 10.1029/2003GB002108.

Lobell, D.B., Bala, G., Duffy, P.B., 2006: Biogeophysical impacts of cropland management changes on climate, *Geophysical Research Letters*, **33,** L06708, doi:10.1029/2005GL025492.

Lobell, D.B., and C. Bonfils, 2008: The Effect of Irrigation on Regional Temperatures: A Spatial and Temporal Analysis of Trends in California, 1934–2002, *Journal of Climate*, **21,** 2063–2071.

Lobell, D.B., C. Bonfils, and J.M. Faurès, 2008: The Role of Irrigation Expansion in Past and Future Temperature Trends, *Earth Interactions*, **12**, 1–11.

Mahmood, R. and Hubbard, K.G., 2002: Anthropogenic land-use change in the North American tall grass-short grass transition and modification of near surface hydrologic cycle, *Climate Research*, **21**, 83-90.

Mitchell, K. and Coauthors, 2004: The multi-institution North American Land Data Assimilation System (NLDAS): Utilizing multiple GCIP products and partners in a continental distributed hydrological modeling system, *J. Geophys. Res.*, **109,** D07S90, doi: 10.1029/2003JD003823.

NOAA, 2005: Technical procedures bulletin for the T382 Global Forecast System, http://www.emc.ncep.noaa.gov/gc_wmb/Documentation/TPBoct05/T382.TPB.FINAL.htm.

Pinker, R. T. and Coauthors, 2003: Surface radiation budgets in support of the GEWEX Continental-Scale International Project (GCIP) and the GEWEX Americas Prediction Project (GAPP), including the North American Land Data Assimilation System (NLDAS) project, *J. Geophys. Res.,* **108** (D22), 8844, doi:10.1029/2002JD003301.

Ozdogan, M. and Gutman, G., 2008: A new methodology to map irrigated areas using multi-temporal MODIS and ancillary data: An application example in the continental US, *Remote Sensing of Environment*, **112**, 3520–3537.

Ozdogan, M., Salvucci, G.D., and Anderson, B.C., 2006: Examination of the Bouchet–Morton Complementary Relationship Using a Mesoscale Climate Model and Observations under a Progressive Irrigation Scenario, *Journal of Hydrometeorology*, **7** (2), 235–251.

Pielke, R.A. and Zeng, X., 1989, Influence of severe storm development of irrigated land, *National Weather Digest*, **14**, 16-17.

Reynolds, C. A., Jackson, T. J., Rawls, W. J., 2000: Estimating soil water-holding capacities by linking the Food and Agriculture Organization soil map of the world with global pedon databases and continuous pedotransfer functions, *Water Resources Research*, **36** (12), 3653-3662.

Rodell, M., P. R. Houser, U. Jambor, J. Gottschalck, K. Mitchell, C.-J. Meng, K. Arsenault, B. Cosgrove, J. Radakovich, M. Bosilovich, J. K. Entin, J. P. Walker, D. Lohmann, and D. Toll, 2004: The Global Land Data Assimilation System, *Bull. Amer. Meteor. Soc.*, **85** (3), 381–394.

Rogers, E., T. L. Black, D. G. Deaven, G. J. DiMego, Q. Zhao, M. Baldwin, N.W. Junker, and Y. Lin, 1996: Changes to the operational "Early" Eta analysis/forecast system at the National Centers for Environmental Prediction, *Weather Forecasting*, **11**, 391–413.

Segal, M., Pan, Z., Turner, R.W., and Takle, E.S., 1998: On the potential impact of irrigated areas in North American summer rainfall caused by large-scale systems, *Journal of Applied Meteorology*, **37**, 325-331.

Siebert, S., Döll, P., Feick, S., Frenken, K., and Hoogeveen, J., 2007: Global map of irrigated areas version 4.0.1. Rome, Italy: University of Frankfurt (Main), Germany / Food and Agriculture Organization of the United Nations.

Tang, Q., T. Oki, S. Kanae, and H. Hu, 2007: The Influence of Precipitation Variability and Partial Irrigation within Grid Cells on a Hydrological Simulation. *J. Hydrometeor.*, **8**, 499-512.

Thenkabail, P.S., Biradar, C.M., Noojipady, P., Dheeravath, V., Li, Y.J., Velpuri, M., Reddy, G.P.O., Cai, X. L., Gumma, M., Turral, H., Vithanage, J., Schull, M., and Dutta, R., 2008: A Global Irrigated Area Map (GIAM) Using Remote Sensing at the End of the Last Millennium. International Water Management Institute. pp63.

USDA, 2004: Farm and Ranch Irrigation Survey 2003, Volume 3, Special Studies Part 1, Published as a supplement to the 2002 Census of Agriculture, pp216.

Vaughan, P.J., Trout, T.J., and Ayars, J.E., A processing method for weighing lysimeter data and comparison to micrometeorological ETo predictions, *Agricultural Water Management*, **88**, 141-146, 2007.

Weare, B. C. and D. Hui, 2008: Modelling regional climate changes: influences of recent global warming and irrigation in California, *International Journal of Climatology*, **28** (9), 1201-1212.

Yeh, T.C., Wetherald, R.T., and Manabe, S., 1984 Effect of soil moisture on the short-term climate and hydrology change: a numerical experiment, *Monthly Weather Review*, **112**, 474-490.

Figure 1. Geographic patterns of annual irrigation water use ca. 2000 reported by the USGS (top) and modeled in this study (bottom) at the county level in cubic kilometers.

Figure 2. Comparison of irrigation scheme predicted annual water use to the reported values at the county level. The reported data are from the USGS. Note that the data is presented in log scale to show both small and large water use estimates that occur across counties. Each dot represents a county's annual water use in cubic kilometers. Root mean square error (RMSE) and bias of the model results are also shown.

Figure 3. Modeled daily total irrigation amounts (km^3/day) accumulated over the U.S. (black) and three regions: Eastern [95 - 67°W] (blue); Central [110 - 95°W] (green), and Western [124-110°W] (red) U.S. Also shown is the volume of USDA-reported annual irrigation amounts in these three regions for the same year. The bar colors match the colors of time plots.

Figure 4. Difference between simulated monthly evapotranspiration totals (mm/mon) from the *irrigation* and *crops* (19 crops) experiments for May through October (2003).

Figure 5. Growing season (April – October) mean energy budget components (top) and water budget components (bottom) averaged over irrigated areas of the U.S., from the *irrigation* (solid dark color) and *crops* (solid lighter shade) experiments. Energy budget components include latent heat flux (QLE), sensible heat flux (QH), ground heat flux (QG), and net radiation flux

(RNET). Water budget components include precipitation (P: slashes) and irrigation (I: solid), evapotranspiration (ET), total runoff (R), and total column soil moisture (SM). The bottom figure has y-axes for P/I, ET, and R (left) and SM (right). Regions are color coded for all irrigated area (black), Eastern [95 - 67°W] (blue), Central [110 - 95°W] (green), and Western [124-110°W] (red) U.S. irrigated area. All simulations were forced by the same precipitation dataset.

Figure 6. Time series of volumetric soil moisture content (left axis) and daily total irrigation and precipitation (mm/day) at an irrigated (maize) AMERIFLUX site in Mead, Nebraska. The *irrigation* (black line) and *crops* (gray line) soil moisture outputs are from the top layer, 0-10 cm depth, for the pixel containing the field site (55% maize, 20% soy, 19% wheat, and 6% sorghum). Soil moisture observations (black dots) were measured at 10 cm. Open black dots indicate days when irrigation was applied at the field site. The model forcing (NLDAS) precipitation (medium blue bars) is on top of the irrigation amount (light blue bars). Observed precipitation (orange dots) was taken from the automated station data at nearby meteorological station.

Figure 7. Diurnal cycles of latent heat flux (a) and sensible heat flux (b) at the Mead, Nebraska AMERIFLUX site averaged over August, 2003, and evapotranspiration averaged over August, 2004 (c) and August, 2005 (d) at the USDA site near Five Points, California. Plotted are observations (dots) and output from the *crops* (gray line) and *irrigation* (black line) simulations, in units of W/m^2 as well as mm/hr for ET (right axis).

Figure 8. Improvements in land surface temperature prediction errors represented as

$\Delta LST_{model\text{-}obs} = |LST_{crops} - LST_{GOES}| - |LST_{irr} - LST_{GOES}|$. Both GOES data and predictions are averaged over the 13-day period between August 13 and August 25, 2003 at 18 Z. Presence of positive (red) values indicates that the main improvement caused by irrigation is simulated land surface cooling to match observations over the same period. Note that there are differences in non-irrigated areas but these areas are outside the scope of this paper.

Figure 1. Geographic patterns of annual irrigation water use ca. 2000 reported by the USGS (top) and modeled in this study (bottom) at the county level in cubic kilometers.

Figure 2. Comparison of irrigation scheme predicted annual water use to the reported values at the county level. The reported data are from the USGS. Note that the data is presented in log scale to show both small and large water use estimates that occur across counties. Each dot represents a county's annual water use in cubic kilometers. Root mean square error (RMSE) and bias of the model results are also shown.

Figure 3. Modeled daily total irrigation amounts (km³/day) accumulated over the U.S. (black) and three regions: Eastern [95 - 67°W] (blue); Central [110 - 95°W] (green), and Western [124-110°W] (red) U.S. Also shown is the volume of USDA-reported annual irrigation amounts in these three regions for the same year. The bar colors match the colors of time plots.
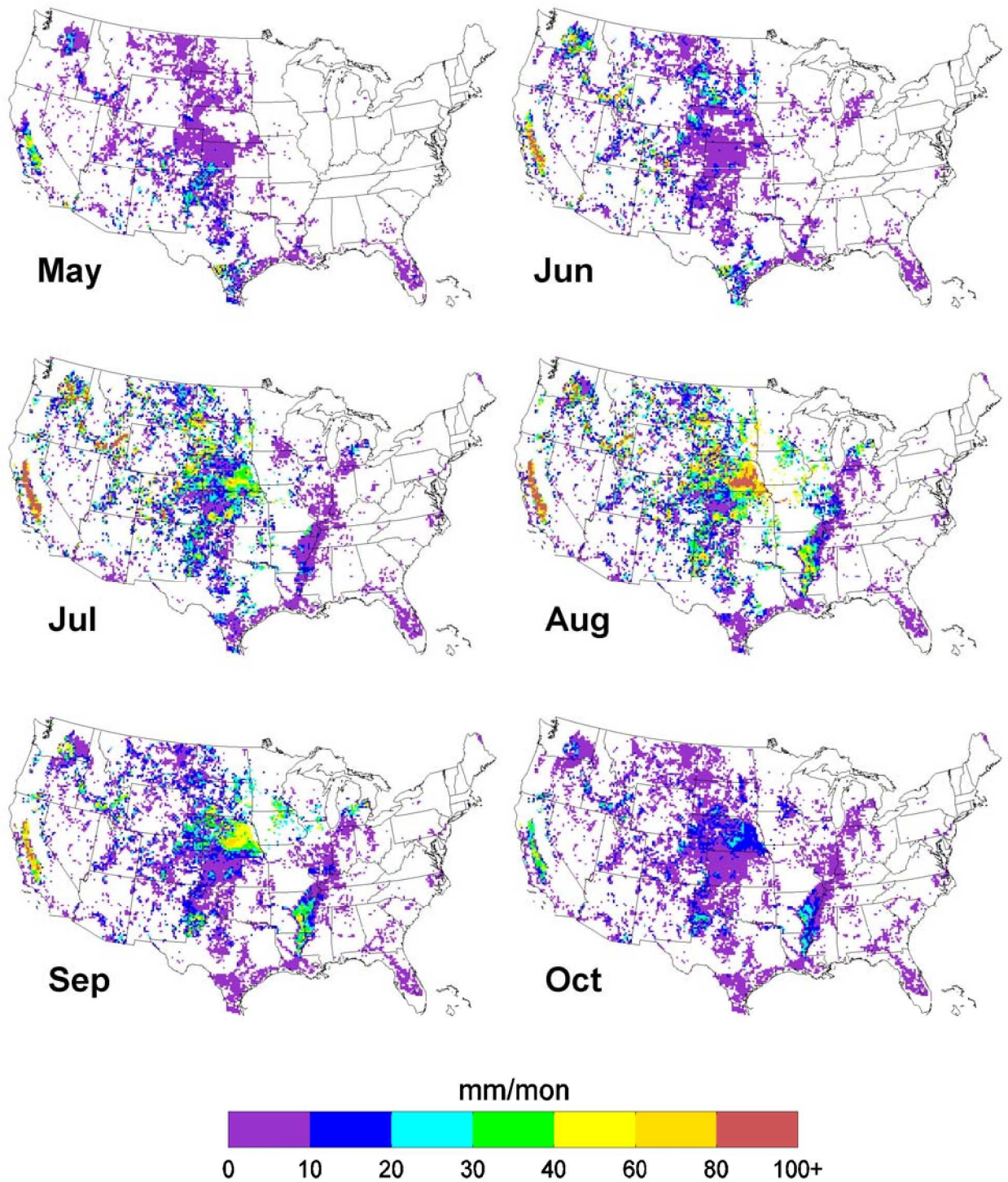
Figure 4. Difference between simulated monthly evapotranspiration totals (mm/mon) from the *irrigation* and *crops* (19 crops) experiments for May through October (2003).
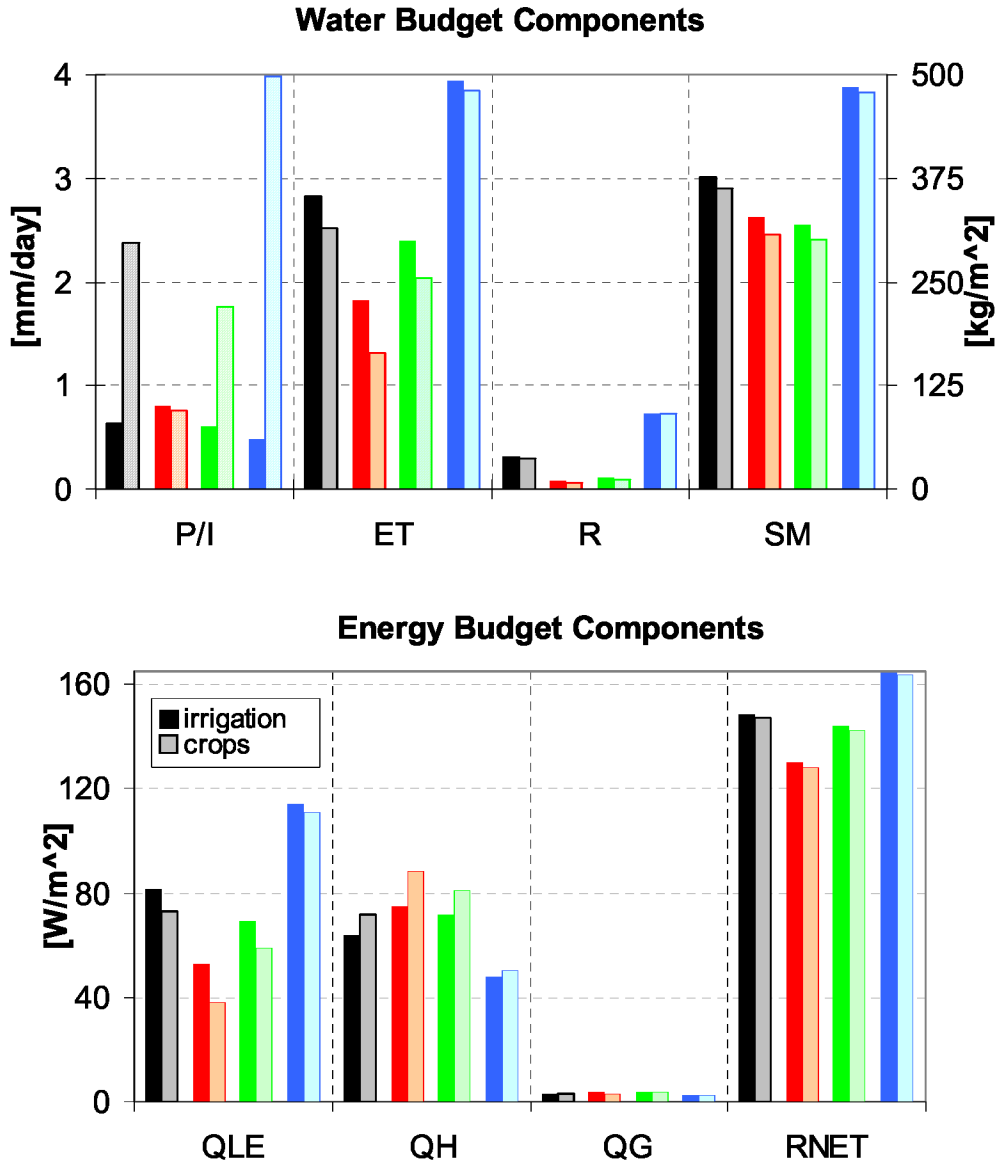
Figure 5. Growing season (April – October) mean energy budget components (top) and water budget components (bottom) averaged over irrigated areas of the U.S., from the *irrigation* (solid dark color) and *crops* (solid lighter shade) experiments. Energy budget components include latent heat flux (QLE), sensible heat flux (QH), ground heat flux (QG), and net radiation flux (RNET). Water budget components include precipitation (P: slashes) and irrigation (I: solid), evapotranspiration (ET), total runoff (R), and total column soil moisture (SM). The bottom figure has y-axes for P/I, ET, and R (left) and SM (right). Regions are color coded for all irrigated area (black), Eastern [95 - 67°W] (blue), Central [110 - 95°W] (green), and Western [124-110°W] (red) U.S. irrigated area. All simulations were forced by the same precipitation dataset.
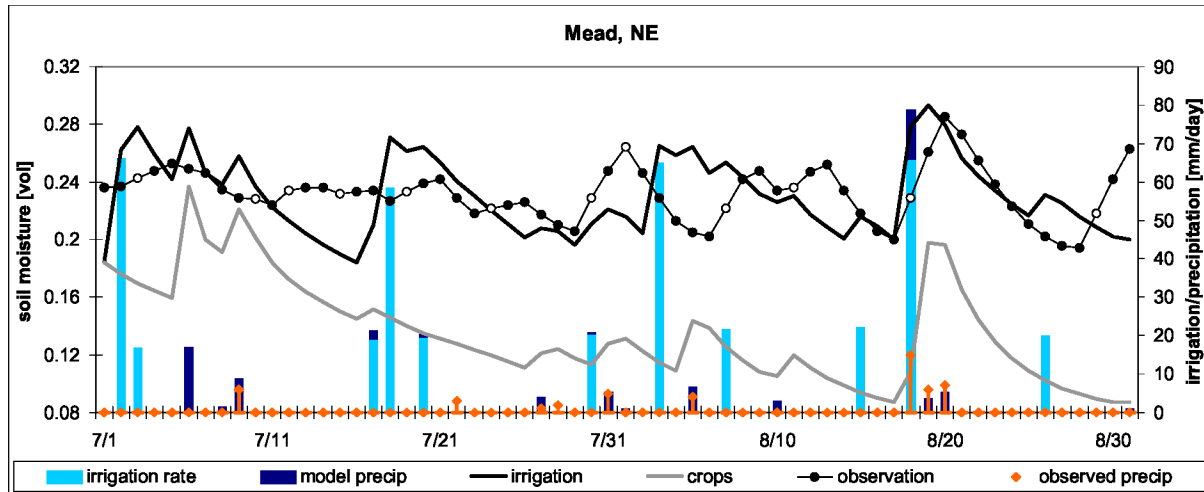
Figure 6. Time series of volumetric soil moisture content (left axis) and daily total irrigation and precipitation (mm/day) at an irrigated (maize) AMERIFLUX site in Mead, Nebraska. The *irrigation* (black line) and *crops* (gray line) soil moisture outputs are from the top layer, 0-10 cm depth, for the pixel containing the field site (55% maize, 20% soy, 19% wheat, and 6% sorghum). Soil moisture observations (black dots) were measured at 10 cm. Open black dots indicate days when irrigation was applied at the field site. The model forcing (NLDAS) precipitation (medium blue bars) is on top of the irrigation amount (light blue bars). Observed precipitation (orange dots) was taken from the automated station data at nearby meteorological station.
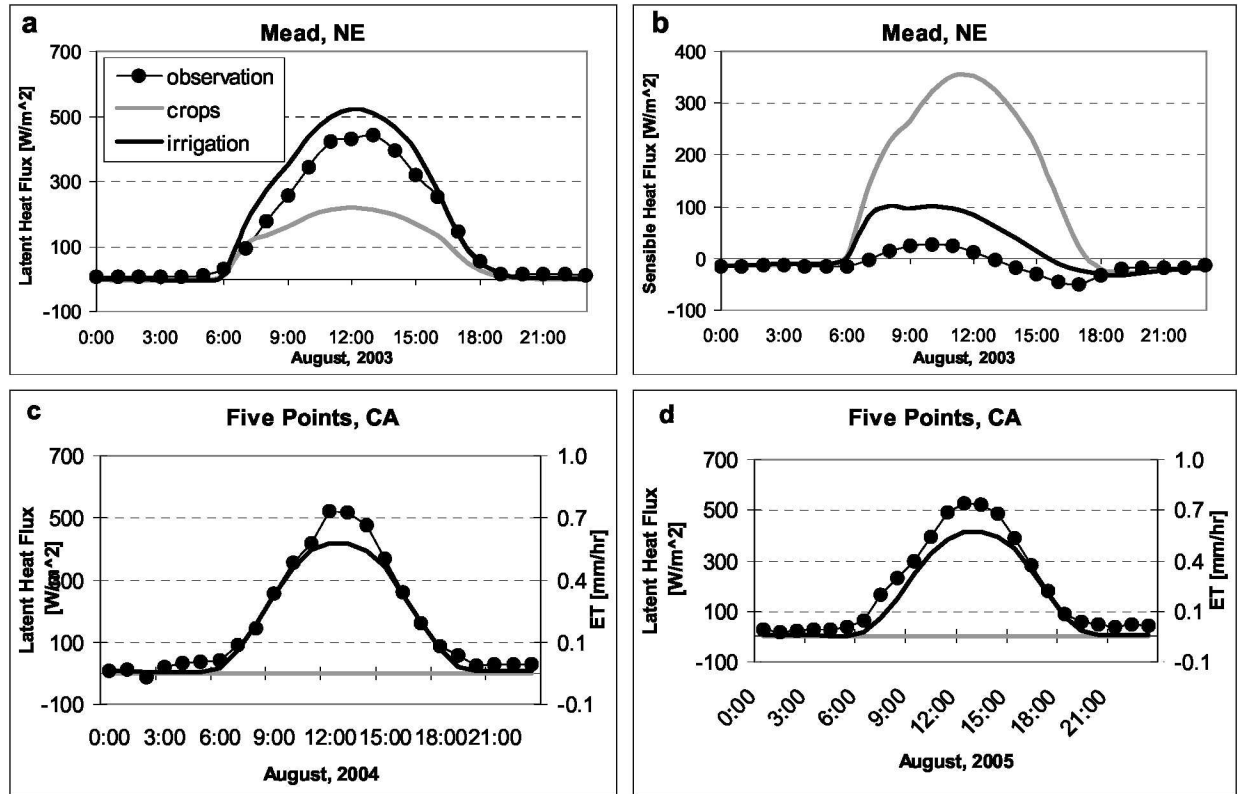
Figure 7. Diurnal cycles of latent heat flux (a) and sensible heat flux (b) at the Mead, Nebraska

AMERIFLUX site averaged over August, 2003, and evapotranspiration averaged over August,

2004 (c) and August, 2005 (d) at the USDA site near Five Points, California. Plotted are

observations (dots) and output from the *crops* (gray line) and *irrigation* (black line) simulations,

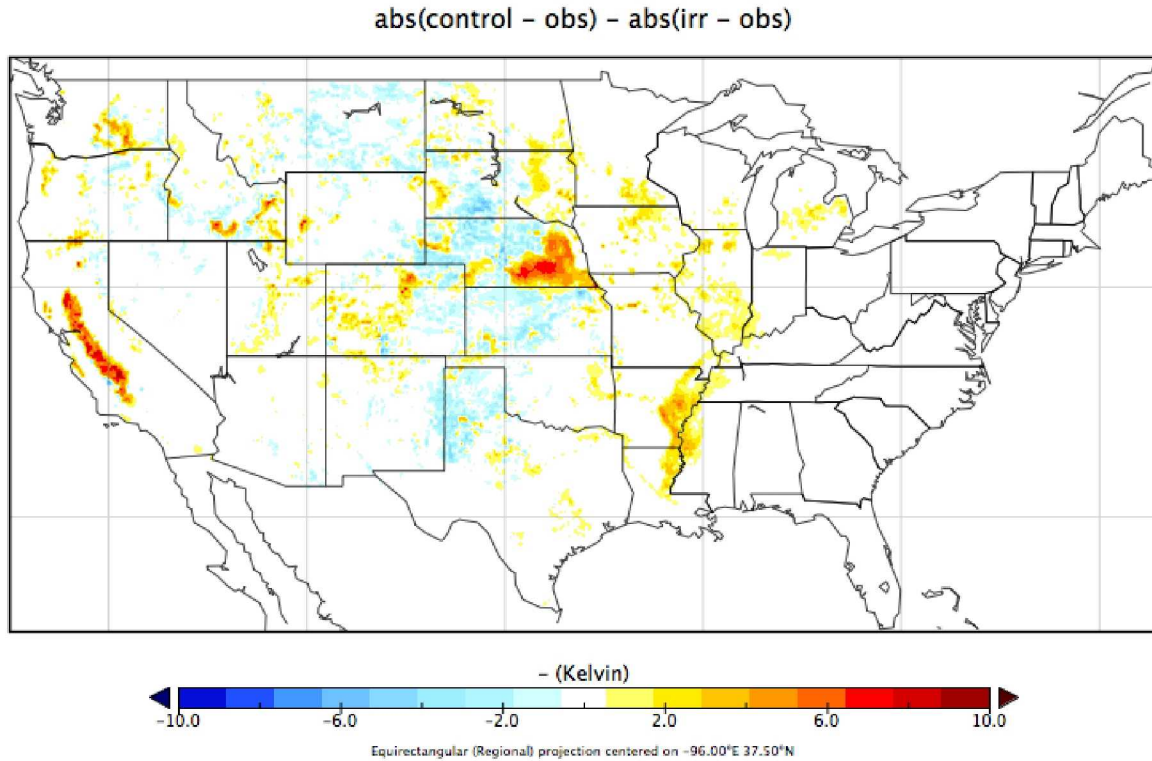in units of W/m^2 as well as mm/hr for ET (right axis).

abs(control − obs) − abs(irr − obs)

Figure 8. Improvements in land surface temperature prediction errors represented as

$\Delta LST_{model\text{-}obs} = |LST_{crops} - LST_{GOES}| - |LST_{irr} - LST_{GOES}|$. Both GOES data and predictions are averaged over the 13-day period between August 13 and August 25, 2003 at 18 Z. Presence of positive (red) values indicates that the main improvement caused by irrigation is simulated land surface cooling to match observations over the same period. Note that there are differences in non-irrigated areas but these areas are outside the scope of this paper.